Subgrid Scale Physics in 1-Month Forecasts. Part I: Experiment with Four Parameterization Packages

J. SIRUTIS AND K. MIYAKODA

Geophysical Fluid Dynamics Laboratory/NOAA, Princeton University, Princeton, New Jersey

(Manuscript received 7 August 1989, in final form 25 November 1989)

ABSTRACT

Four packages of subgrid scale (SGS) physics parameterization are tested by including them in a general circulation model and by applying the four models to 1-month forecasts. The four models are formulated by accumulatively increasing the elaboration and the sophistication of the physics. The first is the reference model (the A-physics); the second model (the E-physics) uses the Monin–Obukhov similarity theory for the fluxes of surface boundary layer, the turbulence closure scheme for the fluxes in the entire atmosphere, and subsurface soil heat conduction; the third model (the F-physics) replaces the cumulus parameterization by the Arakawa–Schubert method; and the fourth model (the FM-physics) enhances the SGS orography. One-month integrations are performed for eight January cases, with each case consisting of three different forecasts. Originally the forecast performance was expected to be a stepwise improvement with the elaboration of the SGS physics from the A to the FM, but the forecast results do not show up in such a simple way. The impact of these processes on the 1-month integration is subtle and yet significant. The superiority of the F-model over the A- and the E-models is evident in the last 10 days of the 1-month forecasts, though the performance of the E-model is consistently good, in comparison with the other models, in terms of root-mean-square (rms) error of geopotential height. It is likely that 80% condensation criterion in the E (instead of 100%) is at least partly responsible for the forecast deterioration in the last 10 days, compared with the F. The FM-model gives the lowest rms error, but the predicted transient eddies are extremely low, probably due to the excessively enhanced orography. The simulated global precipitation patterns are presented for the different models, and the drawbacks are discussed. The F- and the FM-models produce spatially smooth distribution of tropical rainfall. The 30-day forecast performance appears to be more sensitive to the initial conditions, rather than the SGS physics. The systematic errors in all of the models are substantial in magnitude, though they vary with the SGS physics.

1. Introduction

The effects of the subgrid scale (SGS) physics on 1-month forecasts are studied by incorporating various parameterizations into a general circulation model (GCM). Three packages of the SGS physics were suggested by Miyakoda and Sirutis (1977; subsequently referred to as MS1) for the systematic and extensive test of the impact on the GCM forecasts. These packages are referred to as *the A-, the E- and the F-physics.*

The A-physics represents the reference or the control set of parameterizations, which is basically the GFDL (Geophysical Fluid Dynamics Laboratory) 1965 version of the physics package; the E-physics includes sophisticated boundary layer physics and turbulence closure scheme; and the F-physics uses the Arakawa–Schubert cumulus parameterization.

These three physics packages represent a cumulative increase in the sophistication of the subgrid scale physics parameterization. They were regarded in 1977 as reasonably diverse and well defined sets from the standpoint of the concept, as well as the practical formulation, of the respective SGS physics, and therefore, their impact on 30-day forecasts was expected to be clear-cut and sizable. Freezing the GCMs that include these physics, and applying these models to a certain number of sample cases, we planned an intercomparison to investigate the effects and the sensitivities of these parameterizations upon the simulation of atmospheric general circulation and gross weather forecasts.

Preliminary results for four cases were reported in the ECMWF (European Centre for Medium-Range Weather Forecast) workshop on "Convection in Large-Scale Numerical Models," held in December 1983 (Miyakoda and Sirutis 1983; subsequently referred to as MS2), and partially in Smagorinsky's memorial volume (Miyakoda and Sirutis 1985). The present paper is the final documentation on the assessment of these physics, based on 24 monthly runs for eight different January initial conditions.

During the course of this project, Wallace et al. (1983) published an impressive paper that describes a substantial improvement of the medium-range forecast by using "envelope mountains." Accordingly the pres-

Corresponding author address: Mr. Joseph Sirutis, Geophysical Fluid Dynamics Laboratory, P.O. Box 308, Princeton University, Princeton, NJ 08542.

ent research has included this parameterization in the intercomparison. This SGS physics is referred to as *the FM-physics.*

2. Outline

a. The basic GCM

The GCM is the grid-point model with nine vertical levels using the "modified Kurihara" grid in which the Arakawa "A-grid system" is employed (Kurihara and Holloway 1967; Umscheid and Bannon 1977). The horizontal resolution is N48, where N48 denotes 48 grid points between a pole and the equator, corresponding to 1.875° grid size in the meridional direction.

The lower boundary condition is specified by the seasonally varying climatological sea surface temperature.

b. Various SGS physics

The four models are designed to accumulatively increase the elaboration and the complexity in the physics from the A to the FM. The major features of these parameterization packages are listed in Table 1, and brief descriptions are given below.

All of the models have the following in common: large scale condensation; nonlinear horizontal viscosity (Smagorinsky 1963); a simple bucket method soil hydrology in which vegetation is not taken into account; a full radiation package with prescribed noninteractive clouds and no diurnal variation.

The simplest model, the A (Smagorinsky et al. 1965; Manabe et al. 1965) uses the "moist convective adjustment" for cumulus parameterization; dry adiabatic adjustment and a simple mixing length theory are employed to parameterize vertical eddy transports; and the bulk aerodynamic method for thermally neutral stratification is used in the constant-flux layer next to the earth's surface. The condensation criterion is a relative humidity of 80% for both the moist convective adjustment and the large scale condensation.

In the E-model, the vertical eddy transports are replaced by the second order turbulence closure model at 2.5 hierarchy level (Mellor and Yamada 1974, 1982), and the Monin–Obukhov approach based on the similarity theory is used in the constant-flux layer (MS1; MS2). This model contains three subsurface levels for soil heat conduction. The condensation criterion is 80%.

The F-model is the same as the E-model except that the moist convective adjustment is replaced by the Arakawa–Schubert (1974) cumulus parameterization scheme [subsequently referred to as the A–S scheme; see also Lord and Arakawa (1980)]. The planetary boundary layer is modeled by the turbulence closure scheme, as is in the E, and the mixed layer depth is calculated as the "lifting condensation level" (see MS2). The condensation criterion is a relative humidity of 100%. Cumulus friction is also included.

The FM is the same as the F-model except for the use of "2 sigma envelope" orography (Wallace et al. 1983), as opposed to the grid-box-mean orography in the F-model.

Refer to MS1 and MS2 for further information. The details of the models are documented in the internal GFDL manuals on the E-physics and the F-physics.

c. Cases and initial conditions

Eight cases for January 1977–1983 are adopted, and each case is predicted by three initial conditions as stochastic forecasts. These initial conditions are provided by three different analyses that are obtained by the data assimilations of three centers, i.e., the ECMWF, the GFDL, and the NMC (National Meteorological Center). These cases and data are exactly the same as those adopted in Miyakoda et al. (1986).

TABLE 1. The four models of various SGS parameterization packages.

	Features	Remarks	References
A	Moist convective adjustment Dry convective adjustment Drag law formulation of surface fluxes Mixing length theory	GFDL 1965 model 80% condensation criterion	Smagorinsky et al. (1965) Manabe et al. (1965)
E	Turbulence closure model Monin–Obukhov processes Soil heat conduction	No dry convective adjustment 80% condensation criterion	Mellor and Yamada (1974) Miyakoda and Sirutis (1977)
F	Arakawa–Schubert cumulus parameterization	No moist convective adjustment	Arakawa and Schubert (1974) Lord et al. (1982)
FM	Envelope orography	2 sigma envelope	Wallace et al. (1983) Tibaldi (1986)

3. Forecast performance

a. *Simulated general circulation*

The 30-day means of various variables in the models' results are calculated for eight cases and verified by the corresponding observations. The verification data are the NMC analyses. Some highlights are presented here for three variables, i.e., zonal averages of the temperature, the zonal wind, and the sea level pressure (SLP).

1) TEMPERATURE ERROR

Figure 1 is the 8-case mean meridional section of the temperature error, i.e., $T_{\text{pred}} - T_{\text{obs}}$, where T_{pred} and T_{obs} are the temperatures for the prediction and the verification, respectively.

Overall, the error distributions are similar among the four models; the predicted temperature is predominantly lower than the observed. In particular the cold biases are extremely large in the upper troposphere at high latitudes. It is noteworthy that the positive error over the Antarctic is reduced in the E, probably because of the more appropriate surface boundary layer treatment. In the tropics, the F and the FM have a clear warm bias in the upper troposphere centered at 200–250 hPa, compared with the A and the E. This is due to the A–S cumulus parameterization, which gives latent heat release at higher levels than the moist convective adjustment. The A–S scheme has the character of "penetrative convection," whereas the moist convective adjustment scheme operates in the lower unstable layer (see MS1).

Concerning the extreme coldness at high latitudes in the lower stratosphere, it is believed that more effective eddy fluxes are required to transport the tropical heat polewards. This situation can be achieved by an appropriate lateral diffusion which preserves small-scale eddies. This was demonstrated clearly by the $1° \times 1°$ grid 40 level model by Mahlman and Umscheid (1987). Vertical resolution may also be important to eddy heat flux which is associated with vertical phase tilt through the Eliassen–Palm flux.

2) ZONAL WIND ERROR

Figure 2 is the meridional section of the 8-case mean error in the zonal component of the wind. The error distributions of the four models resemble each other, consistent with the distribution of temperature in the context of the thermal wind. The westerly jets are overly intensified, and are shifted poleward in the Northern Hemisphere, and considerably equatorward in the Southern Hemisphere. These features are well-known common shortcomings in almost all GCMs around the world (see Arpe and Klinker 1986; Tibaldi et al. 1987). In the E and in the FM, compared with the A and the F, the errors of jets in the Northern Hemisphere are reduced, but not sufficiently, while the errors in the Southern Hemisphere are increased in the F and even more so in the FM.

A bias toward weaker than observed westerlies over the southern ocean is dominant in all four models.

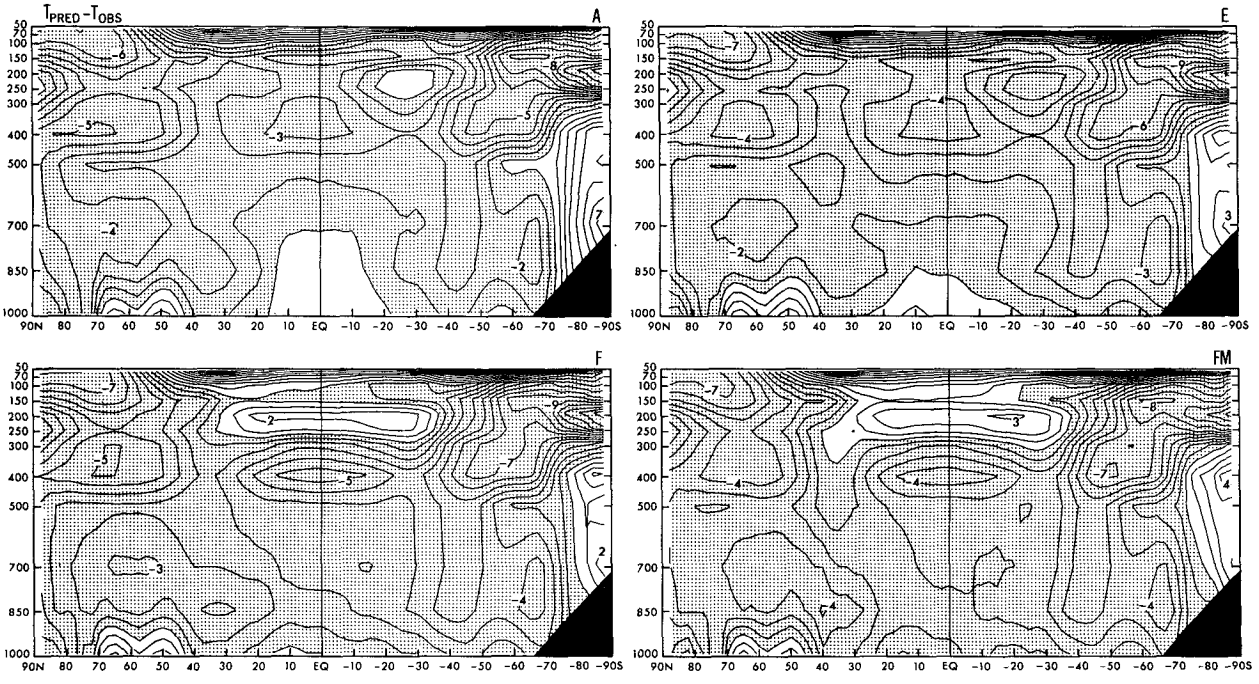

FIG. 1. Temperature errors in the A-, the E-, the F- and the FM-models averaged for all eight cases. The abscissa is latitude, and the ordinate is pressure in hPa. Contour interval is 1°C. The negative regions are shaded.

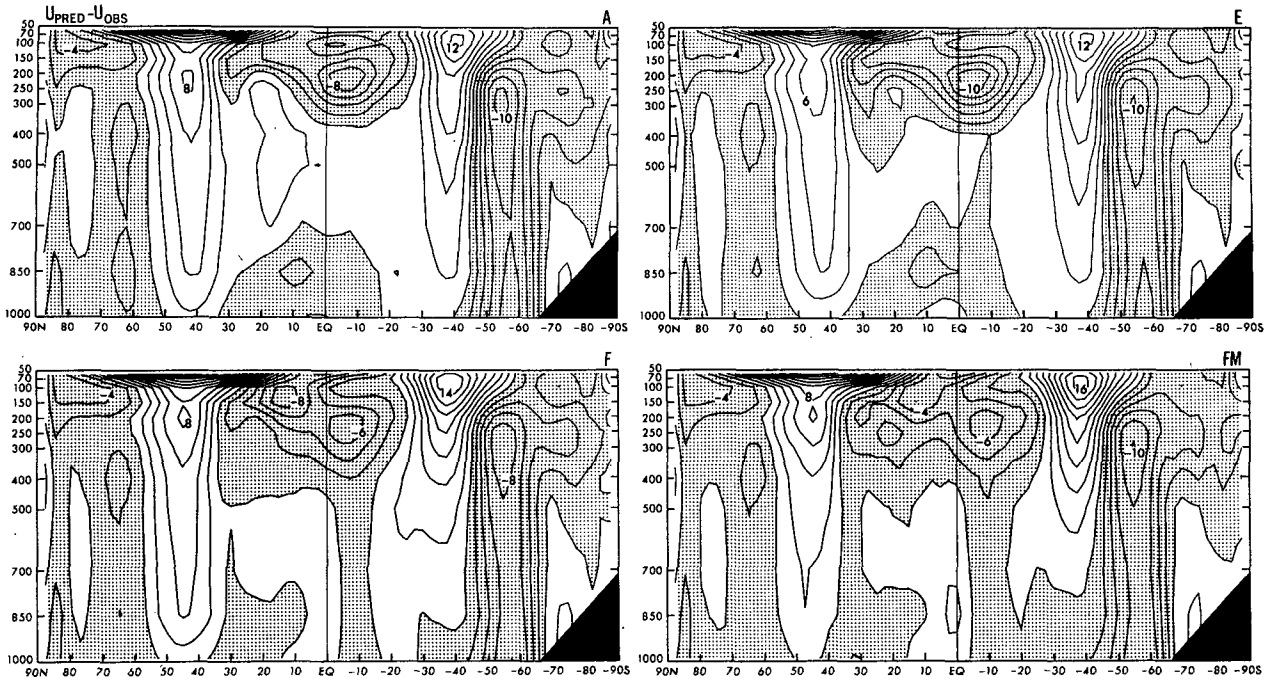

FIG. 2. Same as Fig. 1 except for zonal wind errors. Contour interval is 2 m s^{-1}.

This outstanding feature appears to be consistent with the failure to simulate the low pressure in the Antarctic circumpolar belt, which will be discussed in the next subsection.

In the A and the E models, easterly winds at the upper levels (200 hPa) in the equatorial region are excessively strong. This easterly bias is moderated in the F, possibly due to the "cumulus friction" (Ooyama 1971; Schneider and Lindzen 1976; and Yanai et al. 1982), and even more so in the FM due to the effect of SGS orography.

3) SEA LEVEL PRESSURE

Figure 3 shows the meridional distribution of the 8-case mean SLP for the four models and the corresponding verification.

Clearly, the FM corrected the pressure deficit in the Northern Hemisphere well, but it consequently created another small deficit, which is spread across the tropics. *The largest errors are evident, however, in the Antarctic circumpolar regions.* This tendency is particularly strong in the "modified Kurihara grid" used here.

The failure in the simulation of low pressure in the Antarctic circumpolar regions in other models was pointed out by Gates (1975). This generic problem was thereafter studied by Simmonds (1981), and Mitchell and Hills (1986) in the context of the sea ice extent, the heat flux across the ice surface, and the ice roughness over the southern ocean. It is speculated that vigorous cyclone activities should be present in this belt for the generation of low pressure, and that this situation can only be realized in high resolution models. In the recent high resolution models of the ECMWF and the NMC, for example, the simulation of this low pressure belt was appreciably, but insufficiently, improved (see Tibaldi et al. 1987; Kinter et al. 1988).

b. Systematic errors

The forecast maps of 500 hPa geopotential height, z, are compared with the verifications for the Northern Hemisphere. Figure 4 displays the error maps, i.e., the forecast minus the verification for Days 10–30 averaged, i.e.,

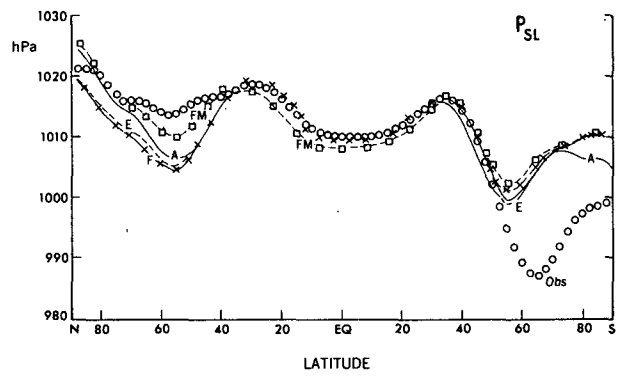

FIG. 3. Latitudinal distribution of sea level pressure averaged for all eight cases. Small circles are the observations. —— A, - - - E, —×—×— F, and —□—□— FM.

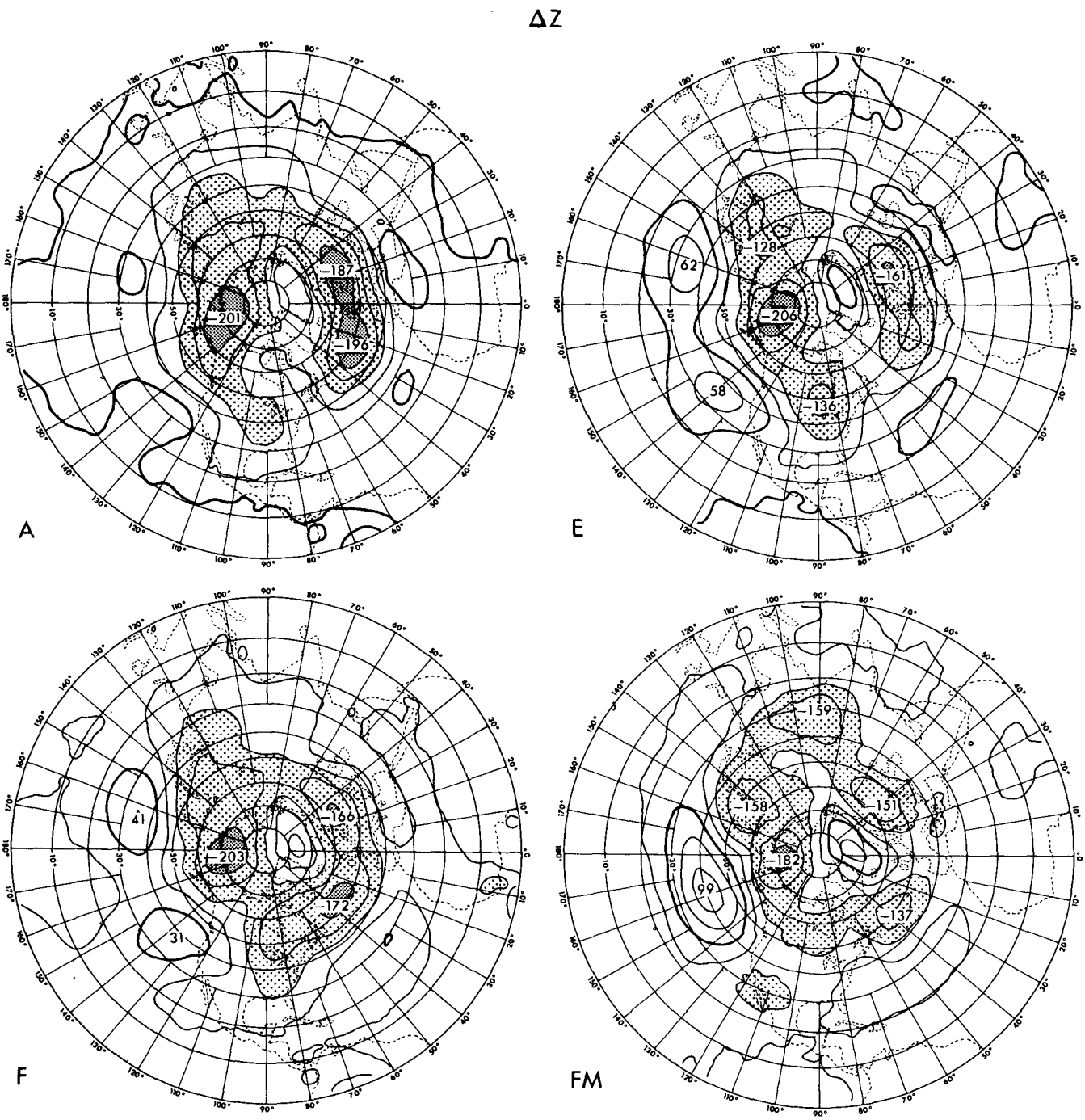

FIG. 4. Arithmetic means of the 500 hPa height errors over Days 10–30 in the four models. Contour interval is 40 m. The areas of error between −80 m and −160 m are lightly stippled, and areas of errors exceeding −160 m are heavily stippled. The plotted values indicate the maxima or the minima.

$$\Delta\langle z\rangle = \langle z_{\text{pred}}\rangle - z_{\text{obs}}, \tag{3.1}$$

$$\text{error} = E(\Delta\langle z\rangle), \tag{3.2}$$

where z_{pred} and z_{obs} are the geopotential heights for the prediction and the verification, respectively, and $\langle\ \rangle$ denotes the arithmetic average over three stochastic forecasts, and E is the ensemble average over eight January cases.

These error maps represent examples of the systematic errors (*climate drift*) for the respective models:

$$(\Delta z)_{\text{drift}} = E\langle z_{\text{pred}}\rangle - z_n, \qquad (3.3)$$

where z_n is the observed norm, given by

$$z_n = E(z_{\text{obs}}).$$

The magnitudes of the error for 500 hPa height (mean absolute values) are in increasing order: the FM, the F, the E, and the A.

In summary, one of the noteworthy points is that *the systematic biases are by and large similar among the various SGS physics (Hollingsworth et al. 1980), and yet differences can be identified.*

c. Forecast errors

The root-mean-square (rms) error of the geopotential height is defined by

$$\text{rms error} = [E(\Delta\langle z\rangle)^2]^{1/2}, \qquad (3.4)$$

which is referred to as the "forecast error." Figure 5 presents the forecast errors for the various models. The errors (mean absolute values) are in increasing order: the FM, the E, the F, and the A. Note the errors over the Aleutian area and the Ural Mountains, which are reduced substantially in the E, compared with the A. It is not clear yet why the large error emerges over the North Atlantic in the F compared with the E. The forecast errors over the Aleutians and the North Atlantic are decreased in the FM.

Comparing Fig. 5 with Fig. 4 shows *a considerable correlation between the two distributions within each model.* This implies that the systematic errors (Fig. 4) constitute the major portion of the forecast errors (Fig. 5). This point was already mentioned in the previous paper (Miyakoda et al. 1986) but only for the E-physics.

Recently Tibaldi and Molteni (1988) have argued that "systematic model errors appear to be mainly produced by the inability of the model to represent the transition between zonal and blocked regimes." In fact, the geographical distribution of the negative error centers in the A, for example, of Fig. 4 agree well with the blocking prone regions. It is, therefore, not implausible that the forecast errors in Fig. 5 are a reflection of the model's inability to simulate blocking. This point will be discussed in a later paper.

d. Skill scores

In order to measure the forecasting skill, the correlation coefficients of the 10-day mean geopotential height anomalies between the forecast and the observation (NMC analysis), and the rms error are calculated for each of eight cases. The verification domain is the Northern Hemisphere (25°–90°N). In calculating the anomalies, a climatological norm for geopotential height obtained by Oort (1983) was used.

Figures 6 and 7 show the scores for 500 hPa height for the eight cases separately. Each case includes 12 curves, which result from three different initial conditions and four different models. As an auxiliary score, the correlations for 10-day mean persistence are displayed in Fig. 6. It is a lag correlation between the 10-day mean height anomaly for the 10 days of the verification period versus Day −10 to 0. The rms error persistence is similarly displayed in Fig. 7. For the persistence verifications, the full field is being persisted.

These figures suggest the following: (i) Quite reasonably, the first 10 days have normally good skill scores, and the later days have less skill, although there are exceptions, i.e., the cases of 1978 and 1980. It is interesting to note that even in these cases the forecast scores for different runs are not entirely random, but they vary with time in a similar fashion. For example, the curves in these cases start with equally poor scores; they later rise and decline together. *The general trend of a model's performance appears to depend upon the circulation regime of the initial condition (Palmer and Tibaldi 1988), rather than small perturbations in the initial conditions.* (ii) The spread of curves among various stochastic forecasts are fairly large in the cases of 1977, 1978 and 1980, and relatively small in the cases of 1982 and 1983, apparently indicating the high sensitivity of forecast scores to the circulation regimes. (iii) The curves generally tend to return to persistence towards the end of the month (Molteni et al. 1986).

In order to investigate the model's performance, the scores are taken separately for each model. Figures 8 and 9 are the results for the ensemble averages of three stochastic forecasts. As it turns out, the case-to-case variability is again dominant in the scores rather than the model's SGS physics (see also Hollingsworth et al. 1980). It is therefore somewhat difficult to extract a systematic feature for different models from these curves.

Figures 10 and 11 are the arithmetic averages of the skill scores for eight January cases with respect to different models. The figures display the scores for the 10-day mean of the forecast and the persistence. In Fig. 11, there is another curve, i.e., the climate (dashed curve); this is the rms difference of the 10-day mean observed height from the norm. Once again in the first 10 days, the scores are high for all cases and for all models. Beyond Day 10, they decay, but not always monotonically, depending upon the models. In the first 10 days, the hierarchy of the performance is, in descending order: *the E, the FM, the F, and the A,* in terms of both the correlation and the rms errors. The difference is subtle in the ensemble mean of eight Januaries, while the difference is substantial in the individual cases of various Januaries.

Beyond Day 10 and up to Day 20, the hierarchy order changes from the first 10 days. The E decays quickly and the F remains high in terms of correlations scores, while the rms error is, in increasing order: *the FM, the E, the F, and the A.* This is the same order as in Fig. 5.

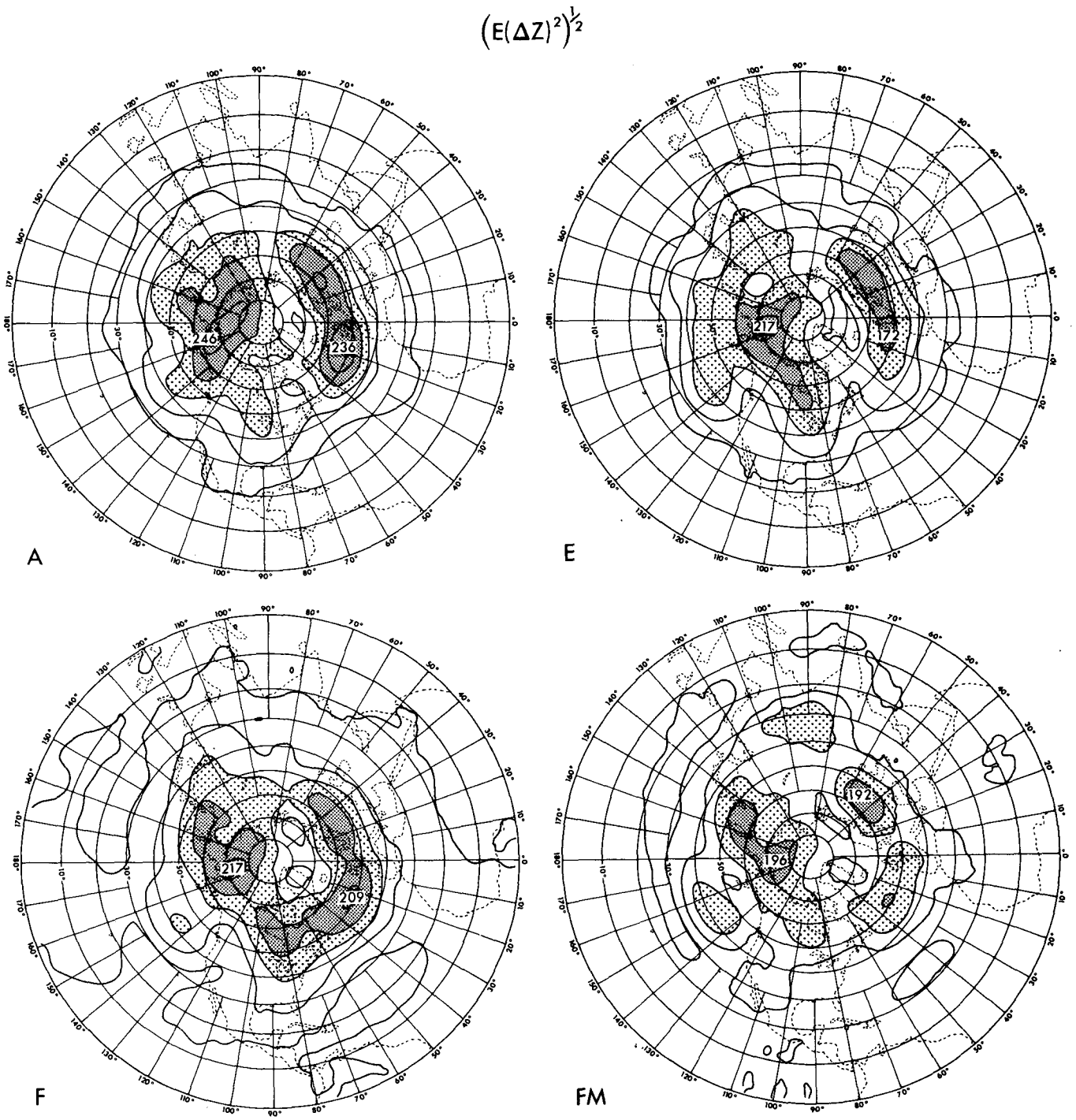

FIG. 5. Rms errors of the 500 hPa height over day 10–30 in the four models. Contour interval is 40 m. The areas of error between 160 and 200 m are lightly shaded, and the areas of error larger than 200 m is heavily shaded. The plotted values indicate the maxima.

Originally it was expected that increasing the sophistication of SGS physics might result in a progressive improvement in the model's simulation. In reality, however, the results are more complex, as is seen in Figs. 10 and 11. In the rms error, the FM is best and the A is worst, and in the correlation scores for the last 10 days, the F and the FM are best. This feature is exactly in the expected order. The E, however, becomes worse than the A in the correlation scores. This disorderly feature needs explanations. We will come back to this point later.

The figures also include the scores of the climate

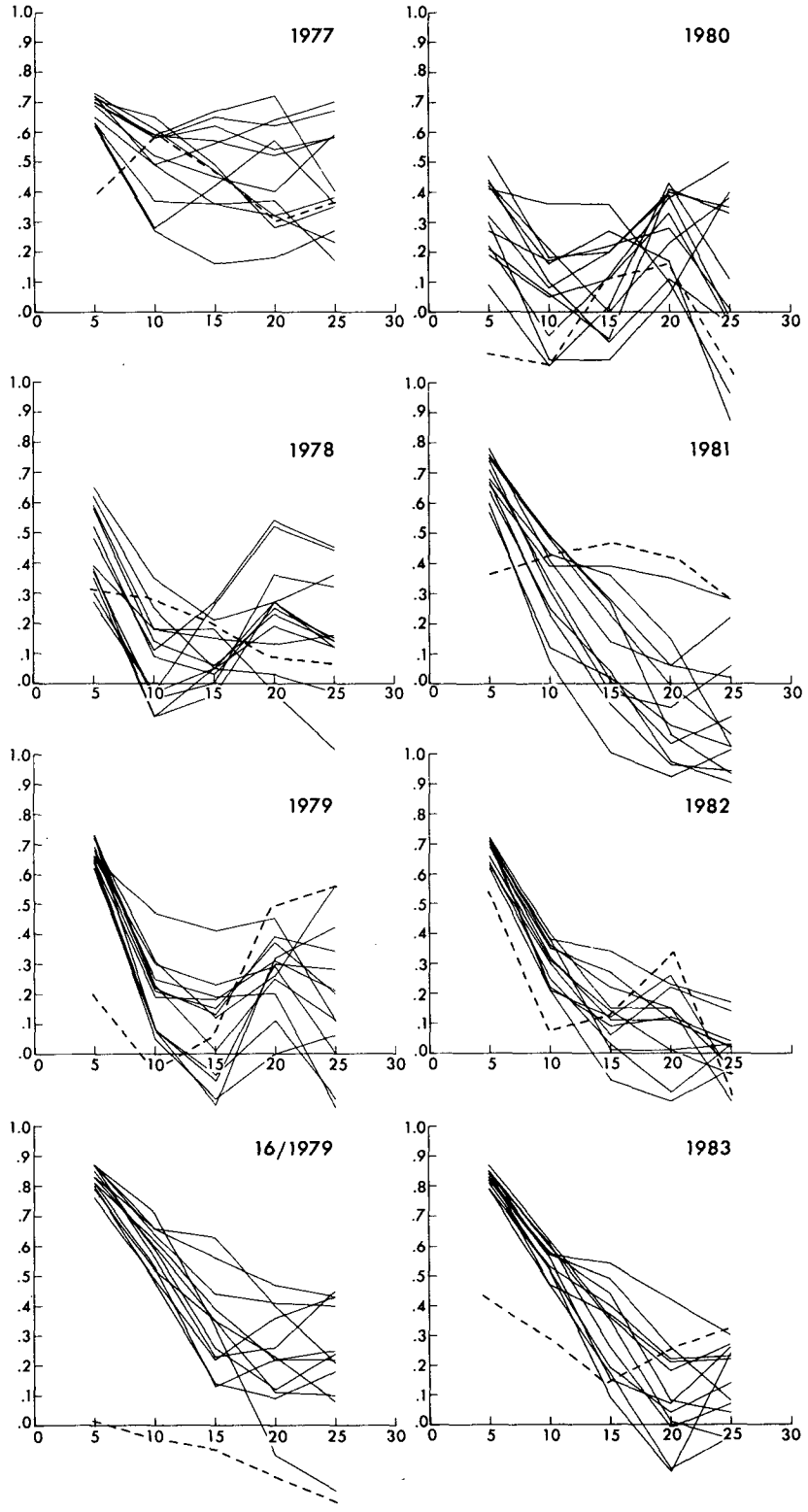

FIG. 6. Correlation coefficients for the 10-day mean of the 500 hPa height anomalies in the eight January cases. The abscissa is the forecast time range in days, and the ordinate is the correlation. Each January case includes 12 solid lines representing forecasts of four different models and three different initial conditions. Dashed lines indicate the 10-day mean persistence.

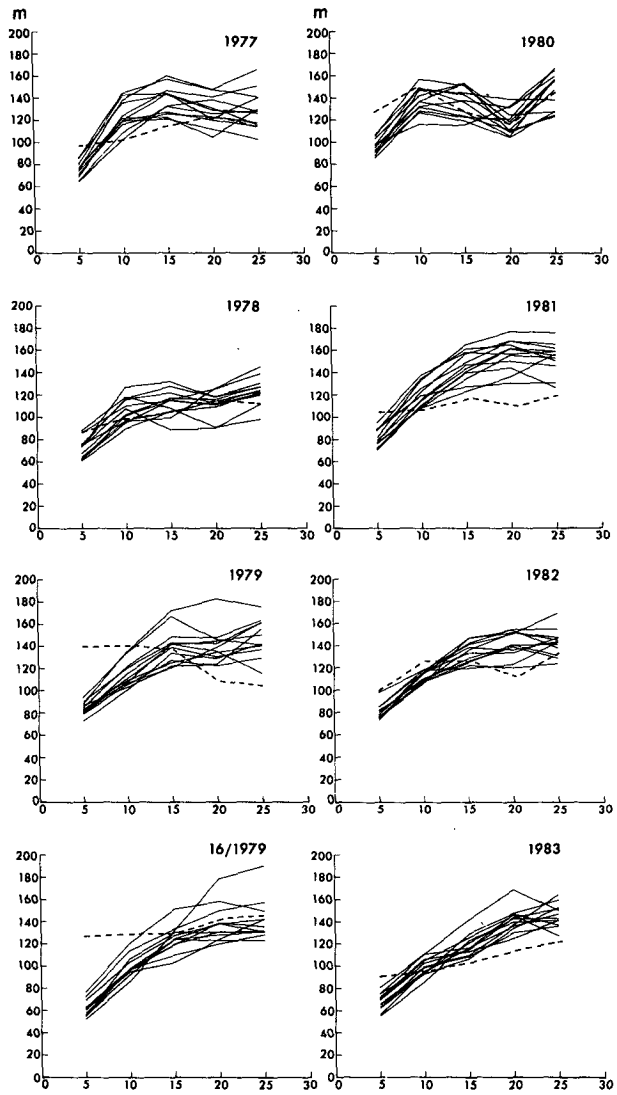

FIG. 7. Rms errors of the 10-day mean of the 500 hPa height. The ordinate is the errors in m. Otherwise same as Fig. 6.

adjusted curves for the selected physics. A climate drift adjustment is made by simply subtracting the systematic error (3.3) for each model from the original forecasted height z (Molteni et al. 1986; Miyakoda et al. 1986). The results of the climate-adjusted curves become more similar to each other among various models (Murphy and Dickinson 1988), apparently implying that the characteristic features tend to be lost due to the elimination of the systematic biases. For simplicity, only two curves, i.e., the E and the F, are shown as examples of climate drift adjustment in Figs. 10 and 11. Note that the systematic error was not calculated from independent data in this paper (see the remarks of Molteni et al. 1986; Hollingsworth et al. 1987; Murphy and Dickinson 1988).

The performance of the FM is somewhat peculiar and erratic. The forecasts deteriorate at Days 15 and 20 in terms of the correlation coefficient, and then become best toward the end of the month. On the other hand, the rms error in the FM are almost always smallest. As will be mentioned later, the forecast fields are overly smooth with the small magnitude of transient kinetic energy. It is therefore considered that the lower rms error in the FM is likely to be due to the lower variability rather than to a better performance (see Molteni et al. 1986). Note that Jarraud et al. (1986) mentioned the detrimental effect for the summer case with the envelope mountain, though the negative effect tends to disappear with increased horizontal resolution.

4. Kinetic energy

From the standpoint of the long-range forecasts, the low frequency variability of the circulation patterns is our particular interest, because only this component has predictability potential. In order to emphasize this component, the monthly mean of circulation fields is calculated. This is referred here to as the time-mean component, and its deviation is called the transient component. In addition, it is customary and also convenient to divide the circulation patterns into the zonal mean and its deviation ("eddy").

a. The notation

Following the Oort (1983) notation, the winds, for example, are divided into the zonal mean, [ ], and the eddy, ( )*, i.e.,

$$u = [u] + u^*, \tag{4.1}$$

or into the monthly mean ("standing"), $\overline{(\ )}$, and its deviation ("transient"), ( )′, i.e.,

$$u = \bar{u} + u'. \tag{4.2}$$

Thus the monthly mean of zonally averaged kinetic energy is written as

$$K = \frac{1}{2}(\overline{[u^2]} + \overline{[v^2]}) \tag{4.3}$$

$$= K_M + K_E, \tag{4.4}$$

where K_M is the zonal mean kinetic energy and K_E is the eddy kinetic energy, i.e.,

$$K_M = \frac{1}{2}(\overline{[u]^2} + \overline{[v]^2}), \tag{4.5}$$

$$K_E = \frac{1}{2}(\overline{[u^{*2}]} + \overline{[v^{*2}]}). \tag{4.6}$$

We next proceed to the decomposition of K_E, i.e.,

$$K_E = K_{SE} + K_{TE}, \tag{4.7}$$

where

$$K_{SE} = \frac{1}{2}[(\overline{u^*})^2 + (\overline{v^*})^2] \tag{4.8}$$

$$K_{TE} = \frac{1}{2}(\overline{[u'^2]} + \overline{[v'^2]}). \tag{4.9}$$

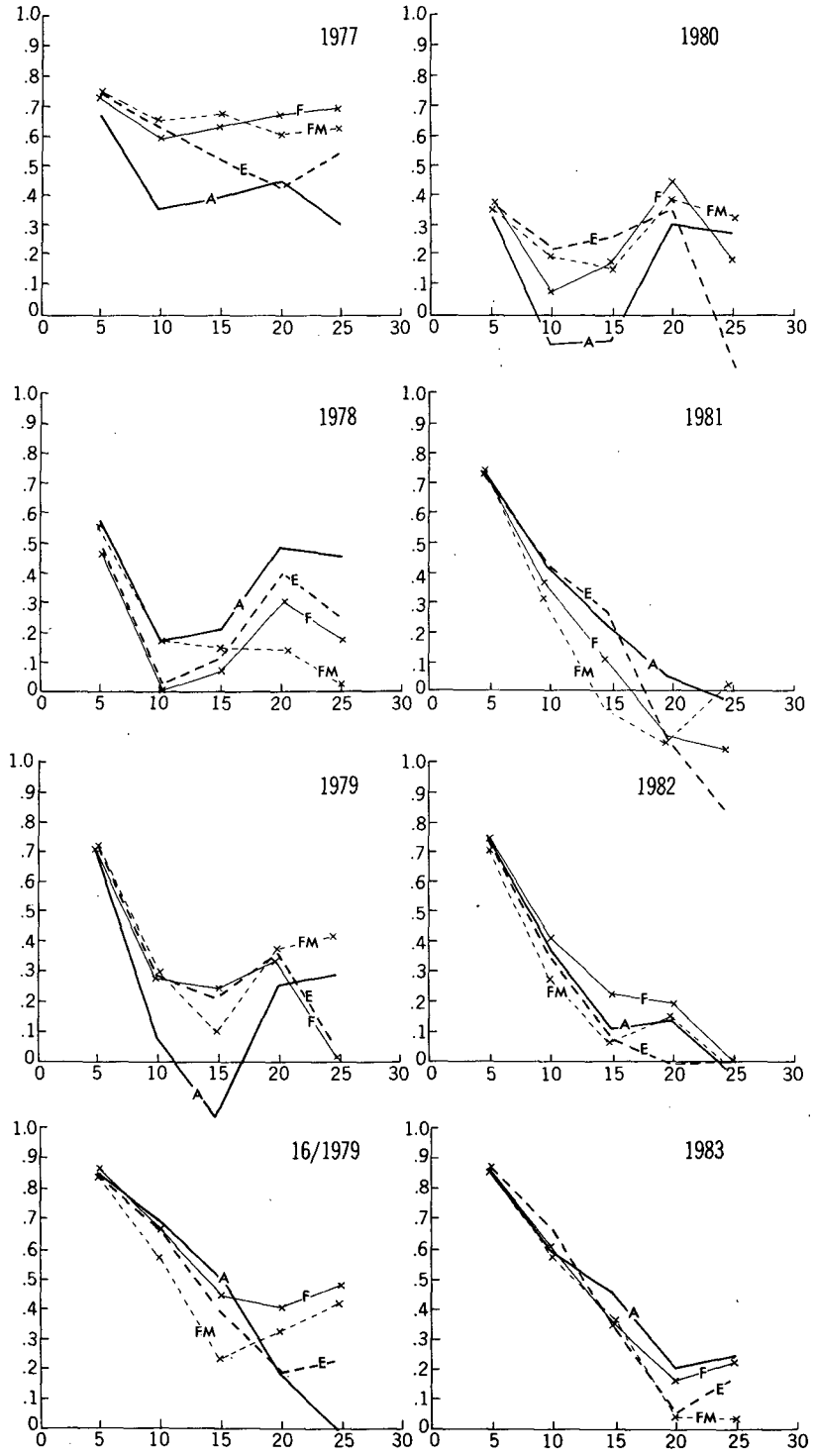

FIG. 8. Correlation coefficients for the same variables as in Fig. 6, except that each January case includes only four solid lines representing the ensemble mean of the three stochastic forecasts for each of the four different models.

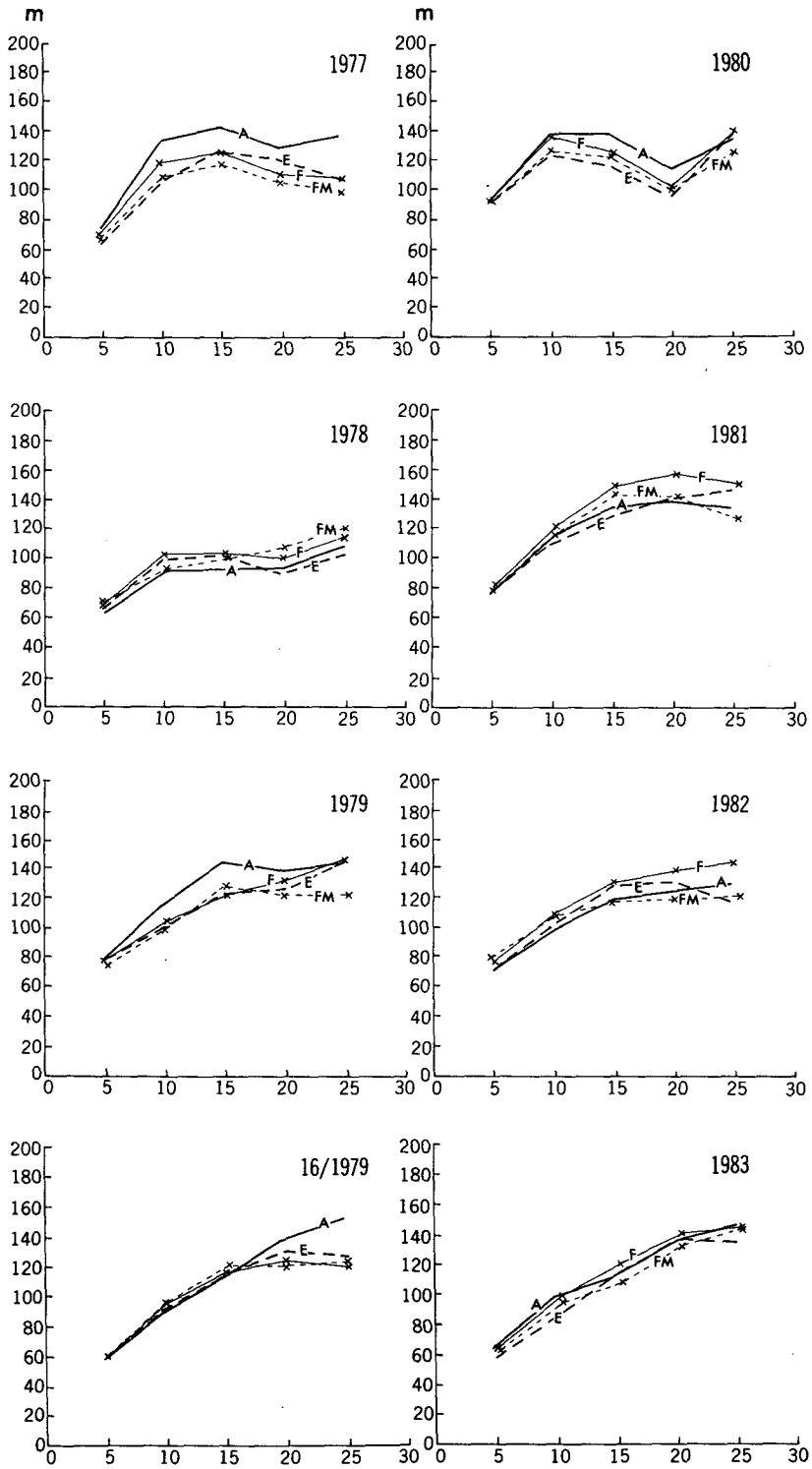

FIG. 9. Rms errors of the same variables as in Fig. 7. See the caption of Fig. 8 for further explanation.

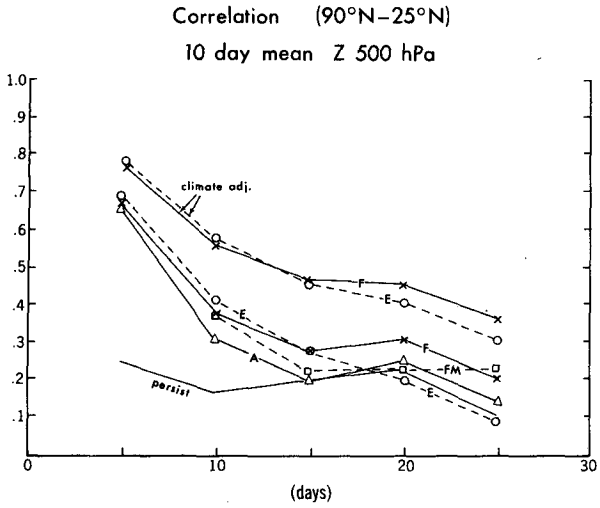

FIG. 10. Ensemble mean correlation coefficients for the four models. The upper curves, marked by climate adjustment, are the scores for the empirically corrected prognosis.

b. *The vertical distribution*

Figure 12 shows the vertical distributions of the zonal mean kinetic energy, K_M, and the eddy kinetic energy, K_E, for the A, the E, the F, the FM and the verification. Both kinetic energies are averaged over the entire Northern Hemisphere for 24 runs of 30 days.

As is seen in this figure, (i) the maximum of K_M at upper levels is located slightly higher than K_E; (ii) the peak of K_M is substantially larger than that of K_E; and (iii) on the other hand, at the lower levels below 500 hPa, K_M is smaller than K_E. These features are in good agreement among the model's simulation, the verification and the climatology (Peixoto and Oort 1974).

The negative aspect of the models' simulation is that (iv) K_E is appreciably underestimated in all models, particularly in the F and even more in the FM; and (v) that the K_Ms in the stratosphere are quite different from the verification, presumably due to the insufficient vertical and horizontal resolution of the models.

Figure 13 shows the decomposition of K_E into K_{SE} and K_{TE}. The spatial, temporal and ensemble averaging is the same as for Fig. 12. It is most striking that K_{TE} *is extremely small in all models,* notably in the F, and even worse in the FM. It is interesting however to note that, concerning K_{SE}, the E, the F and the FM are good, and the A is worse.

5. Precipitation

a. *The zonally averaged rates*

Figures 14, 15 and 16 portray the meridional distributions of zonal mean rainfall for the whole globe, and over land and ocean separately. The rates of rainfall are calculated from the 30-day averages. The January climatological value is taken from Jaeger (1976). The FM is again omitted from the comparison for ease of display; in fact, the results of the FM are similar to those of the F.

The following is noted in these figures. (i) The tropical rain is larger over land than over ocean, whereas the extra-tropical rain is markedly larger over ocean than over land. (ii) The model's rainfall is substantially larger than the climatology (Fig. 14). (iii) The rate of tropical rainfall in the F is closest to the climatology, and that of the A deviates most. (iv) The rate of extratropical rainfall in the F is in best agreement with the climatology except over the Southern Ocean, and the rate of the E shows the largest discrepancy.

In the tropics it is quite evident that the rain in the A is much larger over land than over sea, and that the total amount in the F is closest to that in the climatology, though it is still excessive and is broader in meridional extent. In the extratropics of the Northern Hemisphere, the rates in the E and the A are substantially larger than the climatology. Part of the reason may be the 80% condensation criterion in the A and the E, as opposed to 100% criterion in the F. This possibility is to some extent supported by the results of Manabe and Holloway (1975) who used a scheme similar to that used in A except that the condensation criterion was 100%. Their predicted rainfall is closer to the climatology than in the A prediction in Fig. 14.

A noteworthy point in the above is that the rainfall of the E over the extratropical ocean at 60°N is much larger than that of the A. This deficiency might have a serious impact on the prediction of cyclones and anticyclones in this area. We will examine this in section 6.

We now consider the squared pressure velocity, ω^2, averaged vertically, zonally, and temporally for 30 days,

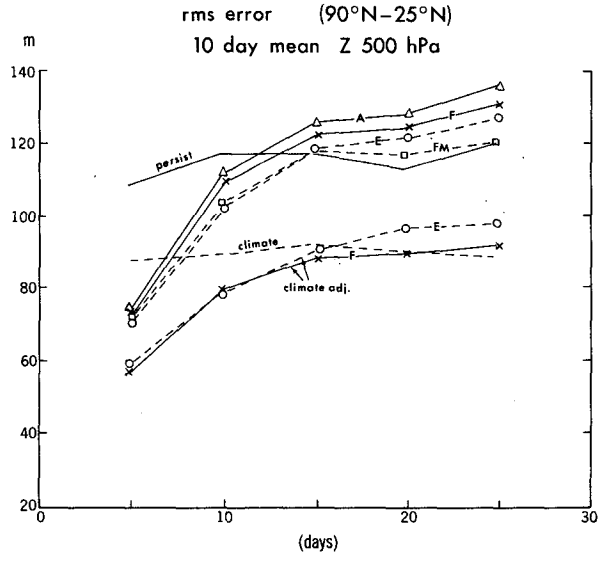

FIG. 11. Same as Fig. 10, except for ensemble mean rms errors.

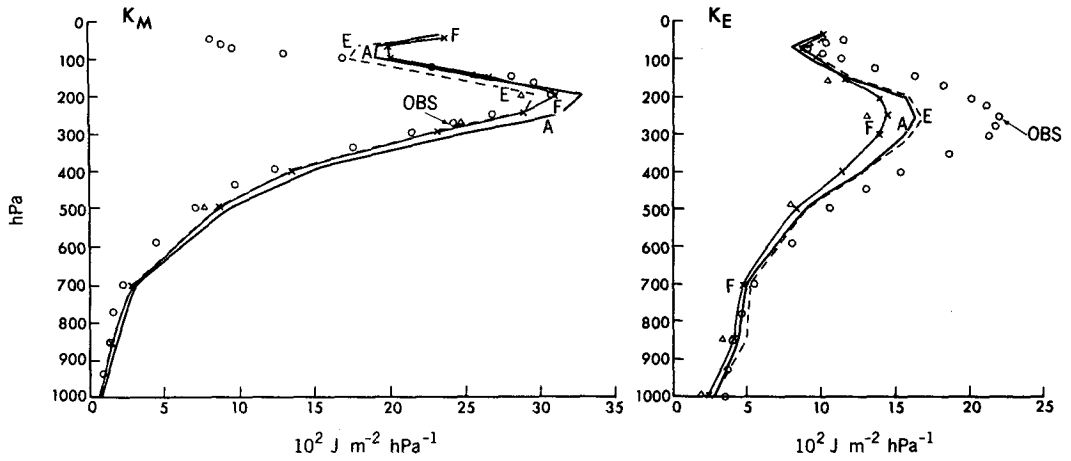

FIG. 12. Vertical distributions of zonal mean kinetic energy, K_M, and the eddy kinetic energy, K_E, averaged over 1 month for the entire Northern Hemisphere. Small circles are observations.

using the twice-daily data, for two cases for each model (Fig. 17). The observation counterpart is not available.

The ω^2 is consistently lowest in the F and the FM (not shown here) compared with the A and the E. The low values of ω^2 in these models are a consequence of the design of the cumulus parameterization. Namely, the A–S scheme is formulated to obtain the slow manifold of cloud mass flux from the dynamical balance of cumulus convection with large-scale environment (Lord et al. 1982), and besides the thermal structure is characterized by the heating-aloft distribution, i.e., more stable stratification, as opposed to the heating-below distribution in the moist convective adjustment.

The A-model generates a strong peak of ω^2 at the equator, and *the E moderates this tendency appreciably.* This feature may be ascribed to the vertical diffusion effect in the turbulence closure scheme and, perhaps more importantly, soil heat conduction in the E, in contrast to the A. The simulation results show that the vertical thermal stratification of the tropical atmosphere in the E is much more stable than the A, as shown in MS2 (see their Fig. 29).

It is interesting to point out that, as is seen in Fig. 14, the order of intensity of ω^2 in various models is consistent with the corresponding rates of precipitation. This is not surprising, because the condensational heating due to cumulus convection induces ω, thus maintaining a good relation between ω and the rate of precipitation. Finally it is noted that the impact of SGS physics or model resolution is most easily identified in ω, and accordingly the Hadley circulation and the rainfall, even if there is no other marked difference (for example, Hollingsworth et al. 1980; Brankovic 1986).

b. *The global distribution*

Maps of precipitation rates are comparatively displayed in Figs. 18 and 19, including the observed cli-

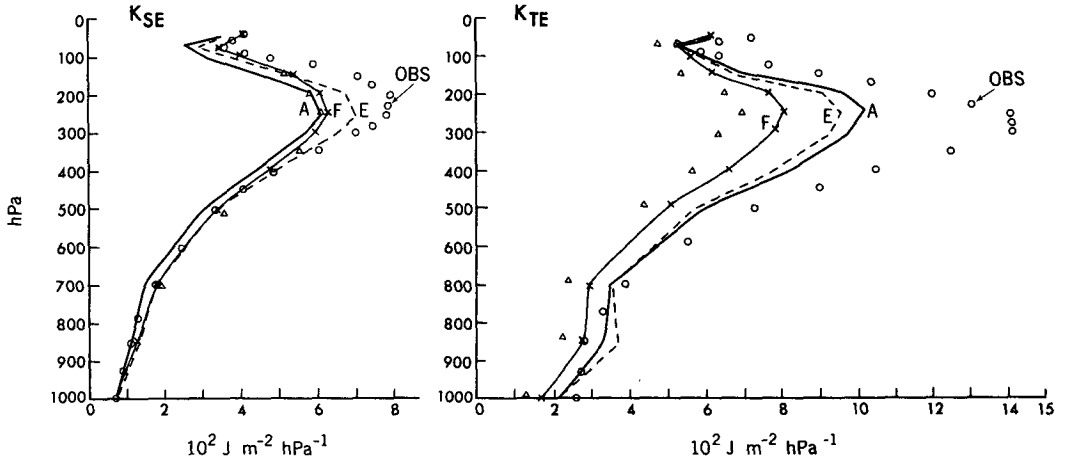

FIG. 13. As in Fig. 12 but for standing eddy kinetic energy, K_{SE}, and transient eddy kinetic energy, K_{TE}.

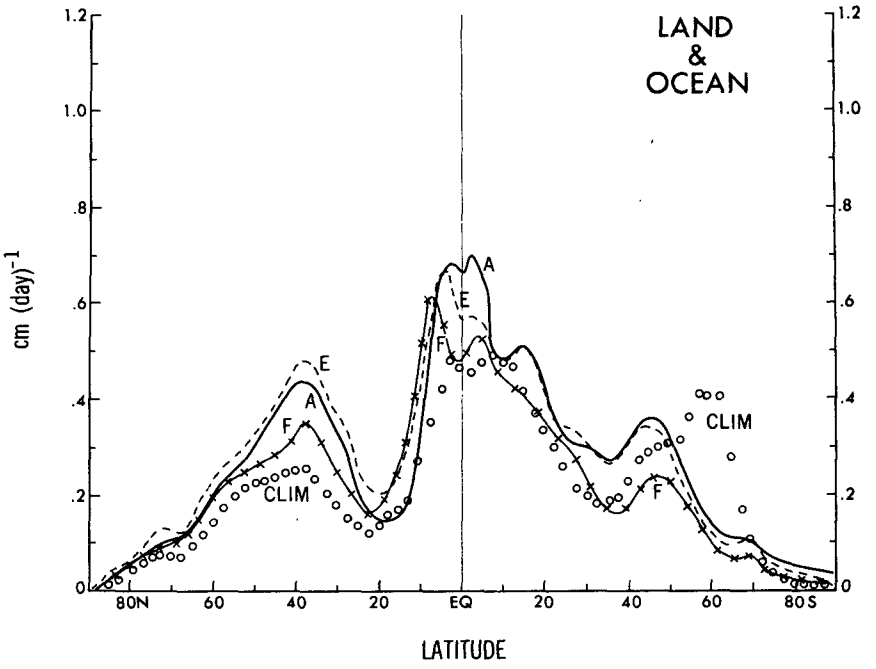

FIG. 14. Latitudinal distributions of zonal mean rates of precipitation, which are averaged over a month for 24 runs, in the simulation of the three models. Units are cm day^{-1}. Small circles are the January climatology of Jaeger (1976).

matologies. The reason why two figures are presented here is that Fig. 18 focuses on the tropical distribution, whereas Fig. 19 stresses the features of the Northern Hemisphere extratropics, using fairly detailed observations.

The maps of global precipitation rates in Fig. 18 include those of the A, the E, the F and the observed January climatology (Möller 1951). The first impression of these distributions are: (i) the major features of observed precipitation are captured by the models

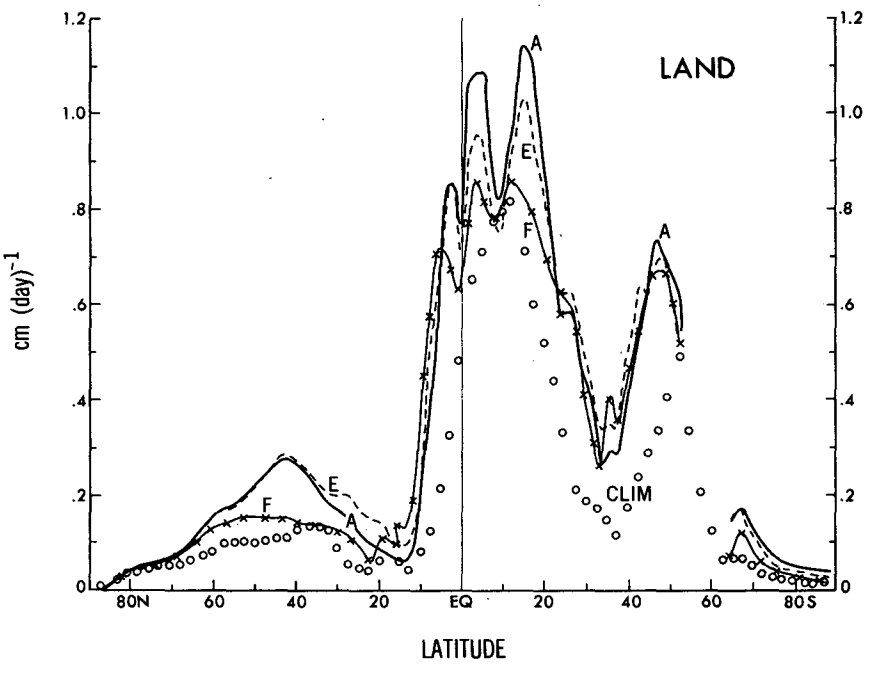

FIG. 15. As in Fig. 14 but only for land.

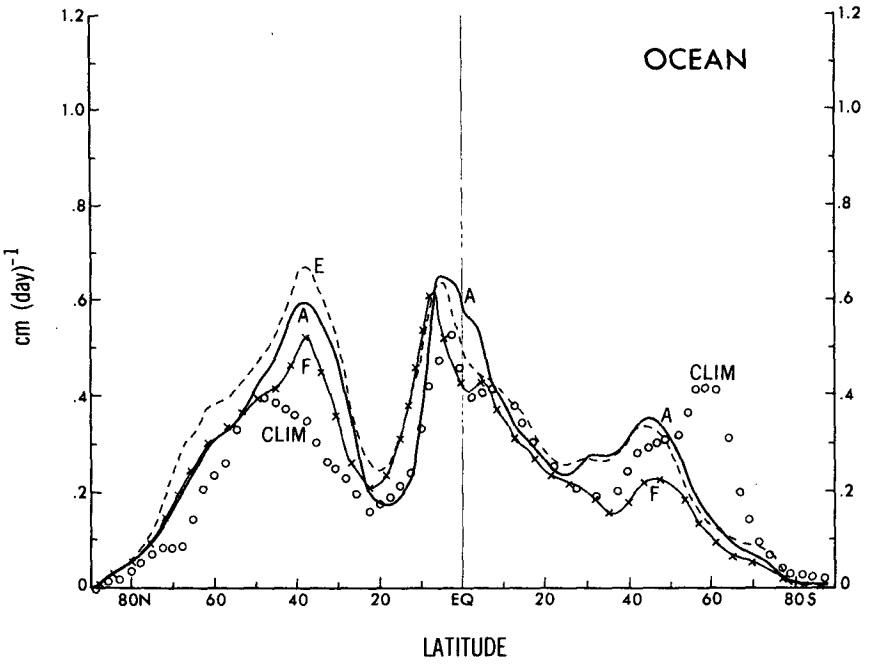

FIG. 16. As in Fig. 14 but only for ocean.

with some exceptions such as the rainfall over the southern ocean; (ii) the model's simulations are remarkably similar to each other, and in some way different from the observed climate distribution; and (iii) the A and the E produce spatially noisy patterns, while the F gives spatially and temporally coherent pattern, though this aspect is not quite evident in Fig. 18, due to averaging over numerous samples.

Some of notable discrepancies of the model's distribution from the observed climatology are summarized below. In tropics, the rainfall over Brazil is excessive in the E and the A, whereas that of the F is in slightly more favorable agreement with climatology. Over the Sahara Desert, there is too much precipitation in all models, while the climate distribution shows essentially no rainfall. Concerning the doldrum zones,

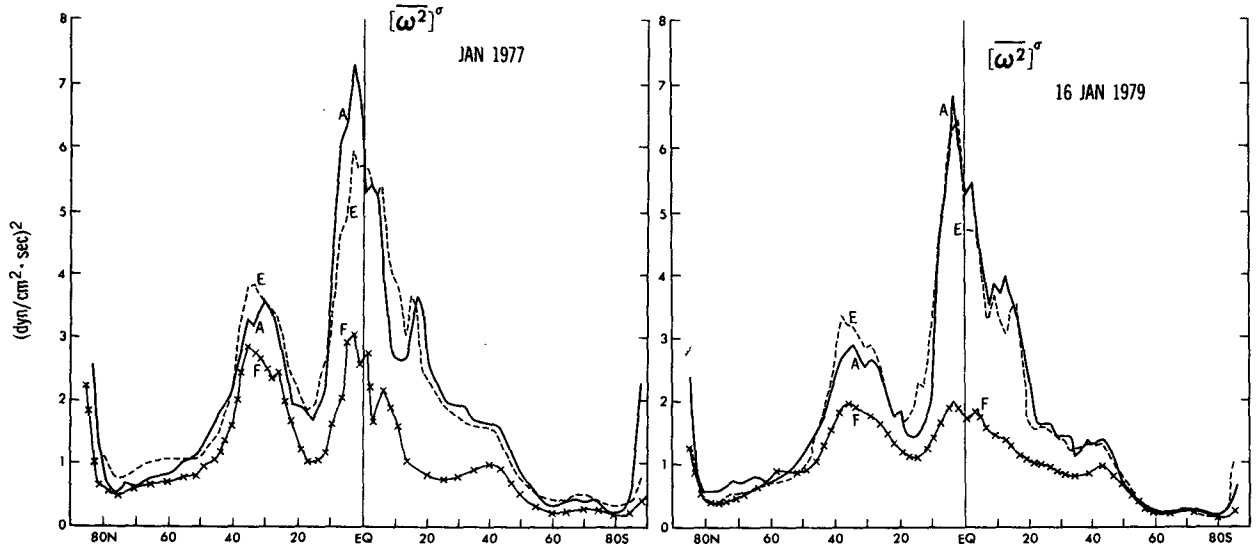

FIG. 17. Latitudinal distributions of zonal mean of squared vertical pressure velocity, ω^2, for two cases, i.e., January 1977 and (16) 1979, averaged over a month.

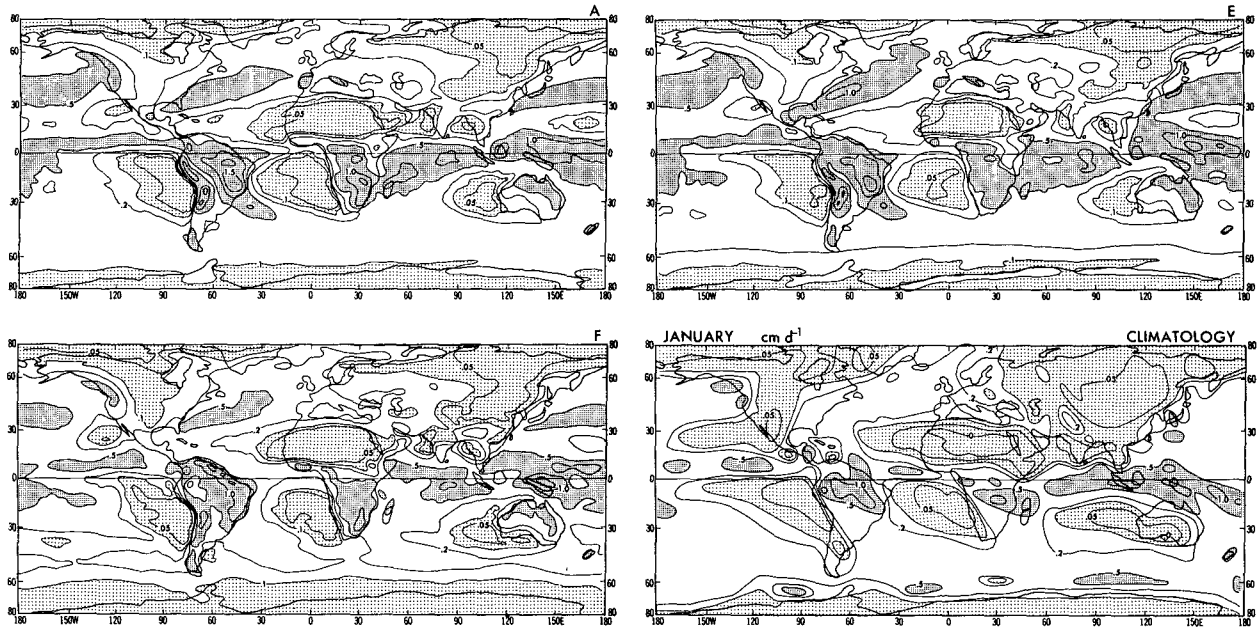

FIG. 18. Global distributions of the precipitation rate by the A-, the E-, the F-models and the January climatology (Möller 1951). The rates in simulations are averaged over a month for the 24 runs. The contours are: 1.5, 1.0, 0.5, 0.2, 0.1, 0.05 and 0 cm day^{-1}. The regions of the rate between 0.5 and 1.5 cm day^{-1} are lightly shaded, and the regions of the rate greater than 1.5 cm day^{-1} are heavily shaded. The regions of the rate between 0.1 and 0 cm day^{-1} are lightly stippled.

which are located to the west of continents, the models fail to produce zonally extended dry areas. The large portion of dry areas in Australia are not well simulated by the A and the E, while there is more, but insufficient, dry area in the F. Other failure in the models' simulation is the erroneous rainfall along the Andes range in all models (see also Kinter et al. 1988; Simmons 1986).

The stereographic map (Fig. 19) for the January climatology, presented by Lvovitch and Ovtchinnikov (1964), exhibits clearly the dry regions at the high latitudes and the doldrums. The F captures the major features, such as the Sahara Desert and the northeast of China, but even the F fails in predicting the poleward protrusion of rainy regions to the east of South China Sea as well as to the east of Venezuela and the Carribean Sea. It also fails in simulating the equatorward protrusion of dry zones to the west of those rainy regions. The ITCZ (Intertropical Convergence Zone) at the eastern equatorial Pacific is inaccurate in the magnitude of precipitation rate for all models, compared with the climatology. Besides the models' ITCZs are shifted too far away from the equator. The result of the FM is not shown here; the pattern of precipitation is similar to that in the F. The deficiencies mentioned above in other models are also present in the FM, except that the dry regions of Mexico and eastern China as well as the China Sea are slightly improved.

One of the merits of the E is to have the Monin–Obukhov scheme, which is supposed to be particularly advantageous over land. In this study, however, so far as the simulated precipitation over land is concerned, the E is no better than the A; in fact, it is worse. The reason might be the inappropriate, oversimplified land surface process, such as the soil moisture treatment (see also Kinter et al. 1988).

c. *The precipitation over the storm tracks*

The maps on the stereographic projection presented in Fig. 19 allow us to inspect the detailed features of the rainfall over the storm tracks. It is striking that the rates of precipitation are seriously overestimated, notably in the E and next in the A, and that the rain belt associated with Atlantic–European storm tracks is too far over central Russia, particularly in the E and to a lesser extent in the A, while the rainfall in the F is modest, and the eastward extension of the rainy region is limited, agreeing well with the climatology. Note that this deficiency in the storm track rainfall in the A and the E is also evident in 100% criterion A-type model (see Manabe and Holloway 1975). The deficient behavior of the E in the later stage of forecast may be explained by the erroneous simulation of storm track precipitation, because the F has substantially better forecast skill in comparison to the E in terms of correlation coefficients.

The question is why the rate of precipitation in the E is erroneously larger than that in the A. One answer for this is the inadequate vertical resolution with the nine levels to define the planetary boundary layer within the framework of the turbulence closure scheme.

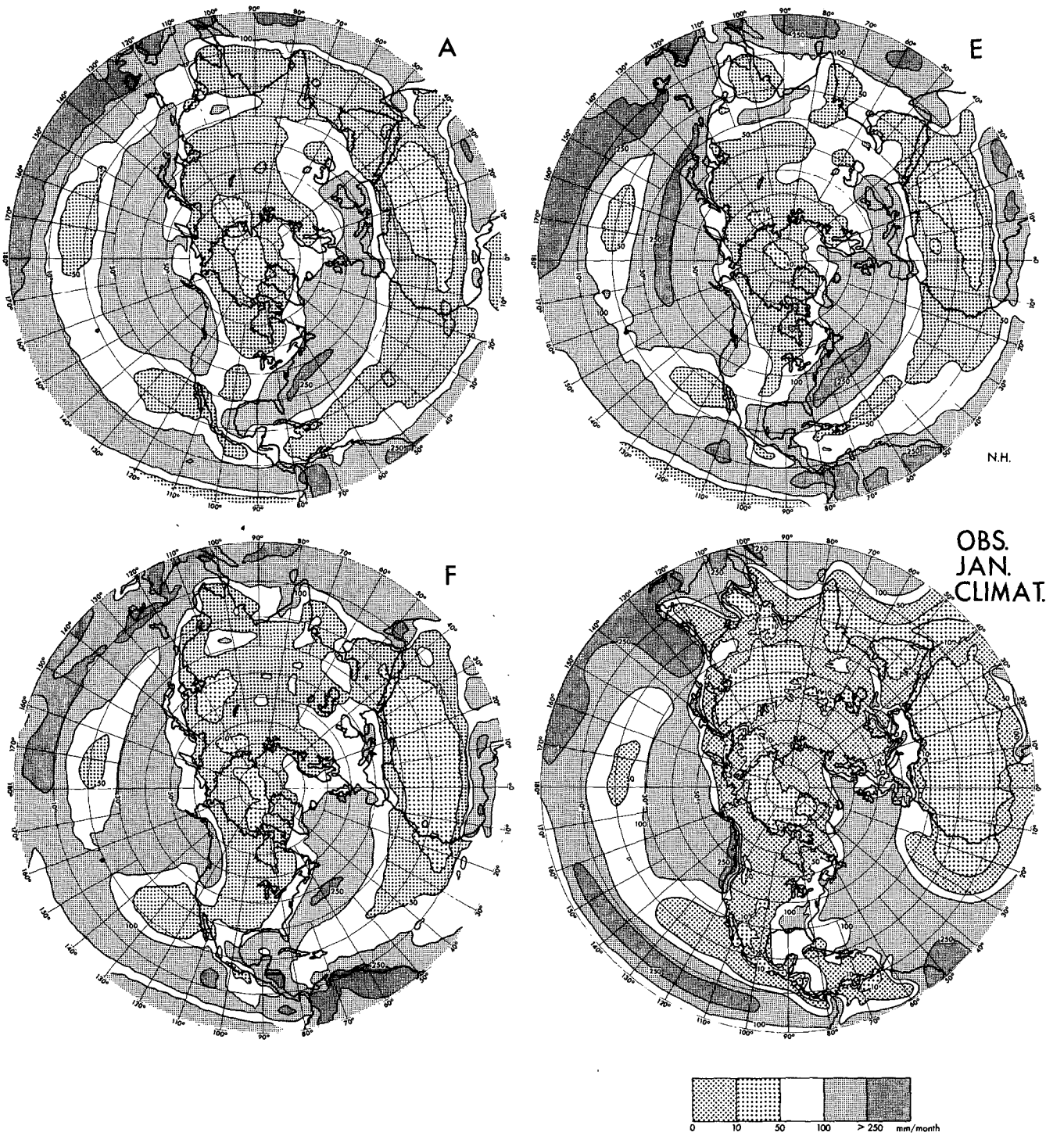

FIG. 19. The rate of precipitation for January (lower right) and forecasts by the A-, the E-, and the F-models. Contours are 500, 250, 100, 50 and 10 mm month^{-1} as shown in the legend.

Manton (1983) mentions that vertical truncation error leads to excessive entrainment and so the mixed layer is a little too warm and dry, and that consequently the vertical eddy transport of latent heat is overestimated. It is possible that these drawbacks might be aggravated by the use of 80% condensation criterion in the E. This speculation has been substantiated by two additional monthly runs, in which 100% criterion is employed in

the E-model. *The amount of precipitation has been substantially reduced in the midlatitude storm track region, and simultaneously the rapid deterioration in correlation scores at the last 10 days of 1-month forecasts in the 1980 and 1981 cases has not shown up.* Note that Hollingsworth et al. (1980) use a more elaborate condensation criterion which is height dependent between 100% and 80%.

Figure 20 shows the zonally averaged distributions of precipitation, evaporation and precipitation minus evaporation for the two cases run with both 80% and 100% condensation criteria. Going from 80% to 100% condensation criteria results in a reduction in both the precipitation and the evaporation rates. There is little change in the difference between precipitation and evaporation at most latitudes, especially in the area of the midlatitude storm tracks.

6. Remarks

Because of the 10-year freeze of the models, the A, the E, the F, and even the FM-physics do not include the most recently developed parameterizations in SGS physics, such as shallow convection and gravity wave drag.

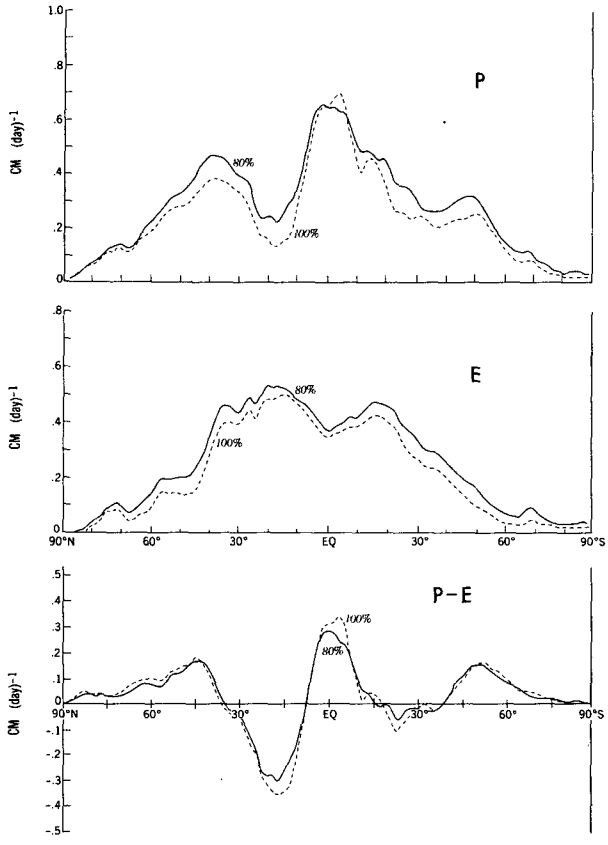

FIG. 20. Latitudinal distribution of zonal mean precipitation (top), evaporation (center), and precipitation minus evaporation (bottom) for the two cases run with both 80% and 100% condensation criteria. The units are cm day^{-1}.

a. *The shortcomings in the present physics and future projection*

The "gravity wave drag" parameterizations associated with the SGS orography (Palmer et al. 1986; McFarlane 1987; Lindzen 1985; Pierrehumbert 1986) is one of the examples of the new parameterization. This parameterization has already been used successfully in reducing the excessive zonal wind at the jetstream level and in the lower stratosphere. This approach appears to be more favorable than the "envelope mountain" in the FM, because the reduction of wind at remote heights is taken into account without the adverse effects on the summer forecasts and the inadequate transient eddy kinetic energy, K_{TE}. The "barrier effect" due to the orography certainly exists, however, and therefore, both effects (i.e., the gravity wave drag as well as the enhanced SGS orography) may be desirable in the GCM parameterization (Pierrehumbert 1986; Miller et al. 1989). According to Tenenbaum (1987), even in the recent prognoses, which include the gravity wave drag parameterization, the excessive forecast winds above the subtropical jet still occur near the Himalayas quite frequently; and this parameterization alone does not appear to cure the deficiency (see also Simmons 1986).

Shallow convection parameterization is another example. In contrast to the deep cumulus clouds, the effect of the shallow nonprecipitating clouds has been underestimated. Tiedtke (1986) was the first to have recognized the importance of this effect for GCMs. Shallow convection has primarily a local effect on the thermal state in the tropics. Water vapor in the trades is accumulated in a cloud layer at the top of the well-mixed boundary layer. The shallow convection plays a crucial role in transporting the moisture and sensible heat from the subcloud layer to the layer above. According to Tiedtke, this convection has a significant effect on atmospheric energetics through intensifying the hydrologic cycle.

When ECMWF included this parameterization in the operational model, there was a marked reduction in the tropical temperature bias in the lower troposphere. Our speculation is that the inclusion of this parameterization in the F may enhance the cumulus convection, and as a result, the K_{TE} may be increased and the Madden–Julian oscillation may be favorably intensified, as will be discussed in the next subsection.

As another interesting revision, Johnson (1976), Kao and Ogura (1987), Frank and Cohen (1987) and others proposed to include the downdraft effect in the A–S scheme. With this effect, the maximum of the cloud mass flux for the shallow clouds is appreciably intensified, and furthermore, both the condensation and evaporation are much more active than in models without downdrafts.

b. Madden–Julian waves

Concerning the A–S scheme, Tokioka et al. (1985) pointed out that the Madden–Julian oscillation or the tropical 40–50-day oscillation is not well represented by this cumulus parameterization. Figure 21 shows the tropical oscillation in the E and the F models in our study. The models were integrated for 120 days, from 1 May to 31 August 1979. The velocity potentials at 300 hPa level are diagnosed, using the technique of Knutson and Weickmann (1987). The results between 5°N and 5°S are shown in the Hovmöller diagram together with the corresponding observation for the same period, i.e., the FGGE analysis of GFDL. Then the wavenumber–frequency analysis of Hayashi (1982) is applied to these model outputs. The results are summarized as follows: (i) Both the E and the F fail in simulating the Madden–Julian oscillation, though all diagrams include eastward propagating waves of zonal wavenumber 1. The waves in the models have substantially greater phase velocities than the FGGE analysis (observation). Hayashi's analysis indicates that the peaks of periodicity are 35 and 22 days in the E; 32 and 17 days in the F, whereas those in the FGGE analysis of both GFDL and ECMWF are 45 and 25 days. (ii) The intensity of velocity potential in the F is extremely weak, i.e., about half of that in the E and less than half of the FGGE analysis. (iii) The E tends to generate the waves of slow speed close to the Madden–Julian waves, but is not successful in maintaining them. According to Hayashi and Golder (1986), the GCM of spectral resolution (R30-rhomboidal truncation at wavenumber 30) with the moist convective adjustment is capable of producing the oscillation of 45- and 25-day periodicities, though the magnitude of the 45-day wave is about half of the counterpart in the FGGE

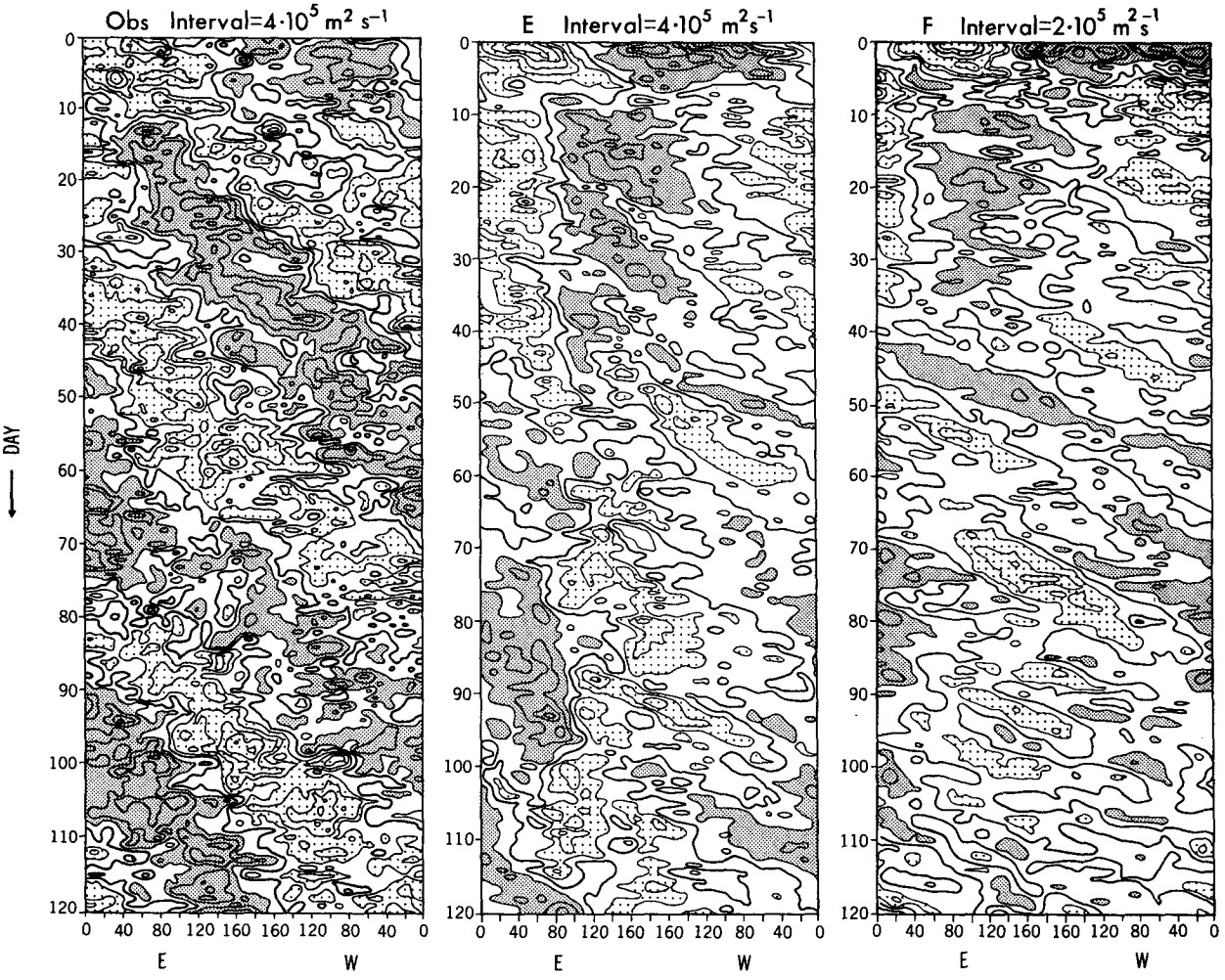

FIG. 21. Hovmöller diagram for time variations of 300 hPa velocity potential (deviation from the 120-day averages at the respective longitude) at 5°N–5°S which are obtained in the E-, the F-models and the FGGE analysis (obs). The thick solid lines are for zero; the regions of potential deviation less than certain negative values are shaded, and the regions of the deviation greater than certain positive values are stippled. Note that the contour interval for the F-model is different from two other diagrams.

analysis. The R15 model failed to generate the Madden–Julian waves.

Note that Tokioka et al. (1988) found that the periodicity of these oscillations is extremely sensitive to the vertical distribution of condensational heating. Based on this diagnosis, they modified the A–S scheme by imposing a constraint on the minimum entrainment rate. In the modified A–S scheme, the 40–50-day oscillation is successfully represented. Overall, the result presented in this paper is consistent with that of Park et al. (1989).

c. *Final remarks*

The impact of the SGS physics is very subtle and delicate. As noted earlier, in the individual forecasts, the circulation regimes have more impact on the prediction performance than does the SGS physics. Consequently, it is extremely difficult to demonstrate that a particular SGS physics is effective for forecasts above the statistical significance level. Nevertheless, modelers have decided to go ahead and incorporate the parameterizations in operational models only on the ground of scientific soundness and based on a limited number of experiments. In most cases, this strategy generally proved to be right. The essence of the incorporation of SGS physics is to push the edge of performance slightly and thereby to attempt at achieving a gradual, and substantial improvement of forecasts. Historically skill scores of forecast have been delicately but steadily raised in many operational centers around the world. It is essential in the future to confront the regime-dependent nature of monthly predictability by taking advantage of the probabilistic forecasts. At present, however, we are not quite ready to use this approach (forecasts of less than about 5 days are all right), because the systematic biases of current models hinder them from simulating all circulation regimes with unbiased probability.

7. Conclusions

Based on the numerical experiments of eight January cases, the simulation performances of the models of four SGS physics are investigated with respect to the 30-day forecasts. The four models, i.e., the A-, the E-, the F- and the FM, are designed to increase progressively the accuracy of the physics from the A- to the FM-model. We expected a stepwise improvement in the models' forecast performance. In reality, however, the results are not so straightforward. To summarize the discussions, the conclusions are drawn as follows:

(i) The 30-day performance appears to be more sensitive to the initial conditions (the circulation regime) more than to the SGS physics.

(ii) The F-, the E- and the FM-models show better performance in the medium-range forecasts of about 10 days, compared with the A-model. The effects are subtle yet substantial.

(iii) The superiority of the F-model over the A- and the E-models is evident during the last 10 days of one-month forecasts, though the performance of the E-model is consistently good in terms of the rms error. The reason why the E decays may be related to the 80% condensation criterion. The reason why the FM-model forecasts deteriorate in certain respects may be the excessive enhancement of SGS orography, resulting in the inferior geopotential height maps, which show unrealistic features, and very weak transient eddy kinetic energy.

(iv) The systematic errors are substantial in magnitude, though they vary with the SGS physics. The FM-model has the smallest systematic error, while the A-model has the largest error. The most prominent systematic errors in the models discussed here are: 1) the westerly jets are overly intensified and shifted poleward in the Northern Hemisphere, and considerably equatorward in the Southern Hemisphere; 2) the temperature is predominantly lower than the observation, the maximum deficit being located in the lower stratosphere at high latitudes; 3) the transient eddy kinetic energy, K_{TE}, is appreciably underestimated in all models, particularly in the FM and the F; 4) the sea level pressure in the Antarctic circumpolar belt (55°S–70°S) is not well reproduced.

(v) Overall, the F-model provides quite realistic zonal mean precipitation rates over ocean and land separately and also the geographical distribution. Some drawbacks are also noticed, however, such as the weak intensity of the resulting transient eddy kinetic energy, particularly in the tropics.

Acknowledgments. The authors are grateful to Drs. J. Smagorinsky and J. Mahlman for their helpful discussions and encouragement in the 10-year study of this work. Gratitude is expressed to Dr. S. Tibaldi, who provided us with the data of "envelope mountain." Thanks are due to Dr. Y. Hayashi and Mr. D. Golder for their help in obtaining the wavenumber–frequency diagrams. The authors also wish to acknowledge the reviews of Drs. C. T. Gordon, Y. Hayashi, J. Katzfey, Y. Kurihara, A. Hollingsworth, and S. Tibaldi. The manuscript was prepared by Ms. W. Marshall and the figures by Mr. P. Tunison and J. Connor.

REFERENCES

Arakawa, A., and W. H. Schubert, 1974: Interaction of cumulus cloud ensemble with the large-scale environment, Part I. *J. Atmos. Sci.*, **31**, 674–701.

Arpe, K., and E. Klinker, 1986: Systematic errors of the ECMWF operational forecasting model in midlatitudes. *Quart. J. Roy. Meteor. Soc.*, **112**, 181–202.

Brankovic, C., 1986: Zonal diagnostics of the ECMWF 1984–85 operational analyses and forecasts. ECMWF Tech. Report No. 57, 72 pp. [Available at European Centre for Medium-Range Weather Forecasts, Shinfield Park, Reading, Berkshire, RG2 9AX England.]

Frank, W. M., and C. Cohen, 1987: Simulation of tropical convective

systems. Part I: A cumulus parameterization. *J. Atmos. Sci.*, **44,** 3787–3799.

Gates, L. W., 1975: Numerical modeling of climatic change: a review of problems and prospects. *Proc. WMO/IAMAP Symposium on Long-Term Climatic Fluctuations,* WMO No. 421, Geneva, World Meteorological Organization, 343–354.

Hayashi, Y., 1982: Space–time spectral analysis and its applications to atmospheric waves. *J. Meteor. Soc. Japan,* **60,** 156–171.

——, and D. G. Golder, 1986: Tropical intraseasonal oscillations appearing in a GFDL general circulation model and FGGE data. Part I: Phase propagation. *J. Atmos. Sci.*, **43,** 3058–3067.

Hollingsworth, A., K. Arpe, M. Tiedtke, M. Capaldo and H. Savijarvi, 1980: The performance of a medium-range forecast model in winter—impact of physical parameterization. *Mon. Wea. Rev.*, **108,** 1736–1773.

——, U. Cubasch, S. Tibaldi, C. Brankovic, T. N. Palmer and L. Campbell, 1987: Mid-latitude atmospheric prediction on time scales of 10–30 days. *Atmospheric and Oceanic Variability,* Cattle, Ed., Roy. Meteor. Soc. Monogr, 117–151.

Jaeger, L., 1976: Monatskarten des Niederschlages für die ganze Erde. *Ber. Deutsch. Wetterdienstes,* **18,** Nr. 139, Offenbach, W. Germany, 38 pp.

Jarraud, M., A. J. Simmons and M. Kanamitsu, 1986: The concept, implementation and impact of envelope orography. *ECMWF Workshop on Observation, Theory and Modelling of Orographic Effects, Vol. 2,* Reading, Berkshire, England, 81–125.

Johnson, R. H., 1976: The role of convective-scale precipitation downdrafts in cumulus and synoptic-scale integrations. *J. Atmos. Sci.*, **33,** 1890–1910.

Kao, C. Y. J., and Y. Ogura, 1987: Response of cumulus clouds to large-scale forcing using the Arakawa–Schubert cumulus parameterization. *J. Atmos. Sci.*, **44,** 2437–2458.

Kinter, J. L., J. Shukla, L. Marx and E. K. Schneider, 1988: A simulation of the winter and summer circulations with the NMC global spectral model. *J. Atmos. Sci.*, **45,** 2486–2522.

Knutson, T. R., and K. M. Weickmann, 1987: 30–60 day atmospheric oscillations: Composite life cycles of convection and circulation anomalies. *Mon. Wea. Rev.*, **115,** 1407–1436.

Kurihara, Y., and J. L. Holloway, 1967: Numerical integration of a nine-level primitive equation model formulated by the box method. *Mon. Wea. Rev.*, **95,** 509–530.

Lindzen, R., 1985: Multiple gravity-wave breaking levels. *J. Atmos. Sci.*, **42,** 301–305.

Lord, S. J., and A. Arakawa, 1980: Interaction of a cumulus cloud ensemble with the large-scale environment. Part II. *J. Atmos. Sci.*, **37,** 2677–2692.

——, W.-C. Chao and A. Arakawa, 1982: Interaction of cumulus cloud ensemble with the large scale environment. Part IV. The discrete model. *J. Atmos. Sci.*, **39,** 104–113.

Lvovitch, M. L., and S. P. Ovtchinnikov, 1964: *Physical-Geographical Atlas of the World.* Academy of Sciences, USSR, and Dept. of Geodesy and Cartography, State Geodetic Commission, Moscow, USSR, 258 pp.

Mahlman, J. D., and L. Umscheid, 1987: Comprehensive modeling of the middle atmosphere: The influence of horizontal resolution. *Transport Processes in the Middle Atmosphere,* G. Visconti and R. Garcia, Eds., D. Reidel, NATO Scientific Affairs Division, 251–266.

Manabe, S., and J. L. Holloway, 1975: The seasonal variation of the hydrological cycle as simulated by a global model of the atmosphere. *J. Geophys. Res.*, **80,** 1617–1649.

——, J. Smagorinsky and R. F. Strickler, 1965: Simulated climatology of a general circulation model with a hydrological cycle. *Mon. Wea. Rev.*, **93,** 769–798.

Manton, M. J., 1983: On the parameterization of vertical diffusion in large-scale atmospheric models. *ECMWF Tech. Report No. 39,* 32 pp. [Available at European Centre for Medium-Range Weather Forecasts, Shinfield Park, Reading, Berkshire, RG2 9AX, England.]

McFarlane, N. A., 1987: The effect of orographically excited gravity-wave drag on the general circulation of the lower stratosphere and troposphere. *J. Atmos. Sci.*, **44,** 1775–1800.

Mellor, G. L., and T. Yamada, 1974: A hierarchy of turbulent closure models for planetary boundary layers. *J. Atmos. Sci.*, **31,** 1791–1806.

——, and ——, 1982: Development of a turbulence closure model for geophysical fluid problems. *Rev. Geophys. Space Phys.*, **20,** 851–875.

Miller, M. J., T. N. Palmer and R. Swinback, 1989: Parameterization and influence of subgrid scale orography in general circulation and numerical weather prediction models. *Meteor. Atmos. Physics,* **40,** 84–109.

Mitchell, J. F. B., and T. S. Hills, 1986: Sea-ice and the antarctic winter circulation, a numerical experiment. *Quart. J. Roy. Meteor. Soc.*, **112,** 953–969.

Miyakoda, K., and J. Sirutis, 1977: Comparative global prediction experiments on parameterized subgrid-scale vertical eddy transports. *Beitr. z. Phys. d. Atmos.*, **50,** 445–487.

——, and ——, 1983: Impact of subgrid-scale parameterizations on monthly forecasts. *ECMWF Workshop on Convection in Large Scale Models,* Reading, Berkshire, England, 231–277.

——, and ——, 1985: Extended range forecasting. *Adv. Geophys.*, **28B,** 55–85.

——, —— and J. Ploshay, 1986: One-month forecast experiments—without anomaly boundary forcings. *Mon. Wea. Rev.*, **114,** 2363–2401.

Möller, F., 1951: Viertel Jahrskarten des Niederschlags für die ganze Erde. *Petermanns Geogr. Mitteil., Justus Perthes, Gotha,* 1–7.

Molteni, F., U. Cubasch and S. Tibaldi, 1986: Monthly forecast experiments with the ECMWF spectral models. *The ECMWF Workshop on Predictability in the Medium and Extended Range,* Reading, Berkshire, England, 47 pp.

Murphy, J. M., and A. Dickinson, 1988: Extended range prediction experiments using an 11-level GCM. *Long-Range Forecasting and Climate Research,* U.K. Met. Office, No. 11, 28 pp., 24 figures. [Available at Meteorological Office, London Road, Brocknell, Berkshire, RG12 2SZ, England.]

Oort, A. H., 1983: Global atmospheric circulation statistics, 1958–1973. NOAA Prof. Paper 14, Rockville, MD, 180 pp.

Ooyama, K. V., 1971: A theory on parameterization of cumulus convection. *J. Meteor. Soc. Japan,* **49,** Special Issue, 744–756.

Palmer, T. N., and S. Tibaldi, 1988: Predictability studies in the medium and extended range. ECMWF Tech. Memo., No. 139, 29 pp., 20 figures. [Available at the European Centre for Medium-Range Weather Forecasts, Shinfield Park, Reading, Berkshire, RG2 9AX, England.]

——, G. J. Shutts and R. Swinbank, 1986: Alleviation of a systematic westerly bias in general circulation and numerical weather prediction models through an orographic gravity wave drag parameterization. *Quart. J. Roy. Meteor. Soc.*, **112,** 1001–1039.

Park, C.-K., D. M. Straus and K. M. Lau, 1989: Intercomparison of interseasonal (30–60 day) oscillations in three general circulation models. *Proc. Thirteenth Annual Climate Diagnostics Workshop,* Cambridge, Massachusetts, Published by Climate Analysis Center/NOAA. [Available at Climate Analysis Center/NMC, 5200 Auter Road, Washington, DC 20233.]

Peixoto, J. P., and A. H. Oort, 1974: The annual distribution of atmospheric energy on a planetary scale. *J. Geophys. Res.*, **79,** 2149–2519.

Pierrehumbert, R., 1986: An essay on the parameterization of orographic gravity wave drag. *ECMWF Workshop on Observation, Theory and Modelling of Orographic Effects, Vol. 1,* Reading, Berkshire, England, 251–282.

Schneider, K. E., and R. S. Lindzen, 1976: A discussion of the parameterization of momentum exchange by cumulus convection. *J. Geophys. Res.*, **81,** 3158–3161.

Simmonds, I., 1981: The effect of sea-ice on a general circulation model of the southern hemisphere. *Sea Level, Ice and Climate Change,* I. Allison, Ed., 193–206. IAHS Pub. No. 131.

Simmons, A. J., 1986: Orography and the development of the ECMWF forecast model. *ECMWF Workshop on Observation,*

Theory and Modelling of Orographic Effects, Vol. 2, Reading, Berkshire, England, 129–163.

Smagorinsky, J., 1963: General circulation experiments with the primitive equations. Part I. The basic experiment. *Mon. Wea. Rev.*, **91,** 99–164.

——, S. Manabe and J. L. Holloway, 1965: Numerical results from a nine-level general circulation model of the atmosphere. *Mon. Wea. Rev.*, **93,** 727–768.

Tenenbaum, J., 1987: Jet stream velocity errors in general circulation models. *Mon. Wea. Rev.*, **115,** 2744–2758.

Tibaldi, S., and F. Molteni, 1987: On the operational predictability of blocking. *ECMWF Workshop on The Nature and Prediction of Extra-Tropical Weather Systems, Vol. II,* Reading, Berkshire, England, 329–371.

Tiedtke, M., 1986: Parameterization of cumulus convection in large scale models. *Physically-Based Modelling and Simulation of Climate and Climate Change.* M. E. Schlesinger, Ed., Reidel, 375–431.

Tokioka, T., K. Yamazaki and M. Chiba, 1985: Atmospheric response to the sea-surface temperature anomalies observed in early summer of 1983: A numerical experiment. *J. Meteor. Soc. Japan,* **63,** 565–588.

——, ——, A. Kitoh and T. Ose, 1988: The equatorial 30–60 day oscillation and the Arakawa–Schubert penetrative cumulus parameterization. *J. Meteor. Soc. Japan,* **66,** 883–901.

Umscheid, L., and P. R. Bannon, 1977: A comparison of three global grids used in numerical prediction models. *Mon. Wea. Rev.*, **105,** 618–635.

Wallace, J. M., S. Tibaldi and A. J. Simmons, 1983: Reduction of systematic forecast errors in the ECMWF model through the introduction of an envelope orography. *Quart. J. Roy. Meteor. Soc.*, **109,** 683–717.

Yanai, M., C.-H. Sui and J.-H. Chu, 1982: Effects of cumulus convection on the vorticity field in the tropics. Part II: Interpretation. *J. Meteor. Soc. Japan,* **60,** 411–424.